

Weakly nonlinear multi-mode Bell-Plesset growth in cylindrical geometry

Hong-Yu Guo(郭宏宇), Tao Cheng(程涛), Ying-Jun Li(李英骏)

Citation: Chin. Phys. B . 2020, 29(11): 115202 . **doi:** 10.1088/1674-1056/ab9c14
Journal homepage: http://cpb.iphy.ac.cn; http://iopscience.iop.org/cpb

What follows is a list of articles you may be interested in

Numerical study on magneto-Rayleigh-Taylor instabilities for thin liner implosions on the primary test stand facility

Xiao-Guang Wang(王小光), Shun-Kai Sun(孙顺凯), De-Long Xiao(肖德龙), Guan-Qiong Wang(王冠琼), Yang Zhang(张扬), Shao-Tong Zhou(周少彤), Xiao-Dong Ren(任晓东), Qiang Xu(徐强), Xian-Bin Huang(黄显宾), Ning Ding(丁宁), Xiao-Jian Shu(束小建)

Chin. Phys. B . 2019, 28(3): 035201 . **doi:** 10.1088/1674-1056/28/3/035201

Coupling between velocity and interface perturbations in cylindrical Rayleigh-Taylor instability

Hong-Yu Guo(郭宏宇), Li-Feng Wang(王立锋), Wen-Hua Ye(叶文华), Jun-Feng Wu(吴俊峰), Wei-Yan Zhang(张维岩)

Chin. Phys. B . 2018, 27(5): 055205 . **doi:** 10.1088/1674-1056/27/5/055205

Rayleigh-Taylor instability at spherical interfaces of incompressible fluids

Hong-Yu Guo(郭宏宇), Li-Feng Wang(王立锋), Wen-Hua Ye(叶文华), Jun-Feng Wu(吴俊峰), Ying-Jun Li(李英骏), Wei-Yan Zhang(张维岩)

Chin. Phys. B . 2018, 27(2): 025206 . **doi:** 10.1088/1674-1056/27/2/025206

Rayleigh-Taylor instability of multi-fluid layers in cylindrical geometry

Hong-Yu Guo(郭宏宇), Li-Feng Wang(王立锋), Wen-Hua Ye(叶文华), Jun-Feng Wu(吴俊峰), Wei-Yan Zhang(张维岩)

Chin. Phys. B . 2017, 26(12): 125202 . **doi:** 10.1088/1674-1056/26/12/125202

Cylindrical effects in weakly nonlinear Rayleigh–Taylor instability

Liu Wan-Hai, Ma Wen-Fang, Wang Xu-Lin

Chin. Phys. B . 2015, 24(1): 015202 . **doi:** 10.1088/1674-1056/24/1/015202

Weakly nonlinear multi-mode Bell–Plesset growth in cylindrical geometry*

Hong-Yu Guo(郭宏宇)[1,2,†], Tao Cheng(程涛)[1,2], and Ying-Jun Li(李英骏)[1,2,‡]

[1] State Key Laboratory for Geomechanics and Deep Underground Engineering, China University of Mining and Technology, Beijing 100083, China
[2] School of Science, China University of Mining and Technology, Beijing 100083, China

(Received 26 April 2020; revised manuscript received 7 June 2020; accepted manuscript online 12 June 2020)

Bell–Plesset (BP) effect caused perturbation growth plays an important role in better understanding of characteristics of the convergence effect. Governing equations for multi-mode perturbation growth on a cylindrically convergent interface are derived. The second-order weakly nonlinear (WN) solutions for two-mode perturbations at the interface which is subject to uniformly radical motion are obtained. Our WN theory is consistent with the numerical result in terms of mode-coupling effect in converging Richtmyer–Meshkov instability. Nonlinear mode-coupling effects will cause irregular deformation of the convergent interface. The mode-coupling behavior in convergent geometry depends on the mode number, Atwood number A and convergence ratio C_r. The $A = -1.0$ at the interface results in larger perturbation growth than $A = 1.0$. The growth of generated perturbation modes from two similar modes at the initial stage are smaller than that from two dissimilar modes.

Keywords: Bell–Plesset effect, Rayleigh–Taylor instability, inertial confinement fusion

PACS: 52.57.Fg, 47.20.Ma, 52.35.Py **DOI:** 10.1088/1674-1056/ab9c14

1. Introduction

Hydrodynamic instabilities in convergent geometries are of great importance for inertial confinement fusion (ICF)[1,2] and astrophysics.[3] It should be noted that nonlinear growth of hydrodynamic instabilities will result in degradation of ICF implosion. For traditional ICF central ignition, a spherical target is imploded inward to achieve the ignition condition and high gain. As the substantial compression of the fuel inside the target is necessary, the convergence ratio C_r of the high-gain target is about ∼30–40, where C_r is the ratio of the initial outer target radius to the final hot-spot radius. The dynamic process of ICF implosion contains four stages, namely, shock transition, acceleration, coasting and deceleration.[4] The shock wave propagates through the perturbed interface in the earlier time, the outer interface of the target is susceptible to the Richtmyer–Meshkov (RM) instability.[5] During the acceleration stage, the shell is imploded to $C_r \sim 2$–3. In the coasting phase, the shell moves towards the center at a constant velocity. There exists significant perturbation growth at the interface which is caused by Rayleigh–Taylor (RT) instability[6,7] and Bell–Plesset (BP) effects[8,9] during the acceleration and coasting stages. As the large C_r is achieved, perturbation growth is magnified by BP effects in the final deceleration stage.

BP effects are considered to be very important for the outcome of ICF implosion experiments,[10–12] cylindrical Z-pinches[13] and converging shock tube experiments.[14,15] The cylindrical convergence on the perturbation growth was first discussed by Bell.[8] Although the motion of a curved interface is absence of acceleration, additional perturbation growth appears, which is quite different from that in the planar case. Plesset[9] considered spherical interface in radical motion with surface tension effect and obtained the similar results. Their results are collectively called the BP effects or BP instability. The RT and BP growths in cylindrically convergent geometry have been measured with Nova lasers,[10,11] perturbation growth at the inner interface due to the convergence effect was observed. Amendt *et al.*[12] further promoted the BP model in a spherical geometry, considering the uniform compressibility of the fluid on both sides of the interface. Epstein analyzed the linear growth of modified RT growth with BP effects and gave a detailed description of RT and BP growths.[16] Velikovich and Schmit[17] investigated the perturbation growth for a finite-thickness shell in both spherical and cylindrical geometries, the time-dependent dispersion equations were obtained. The perturbation amplitude in the converging RM instability was measured in a semiannular shock tube,[15] it was found that BP effect, nonlinear mode-coupling and compressibility were pronounced in the converging cases. The weakly nonlinear (WN) theory has been extensively studied,[18–22] which can be used to describe the formation of spike-bubble structure and mode-coupling process. The third-order WN solutions were derived by Wang *et al.*[22] for a uniformly convergent cylinder. Recently, the WN growths of coupled RT

*Project supported by the Fundamental Research Funds for the Central Universities, China (Grant No. 2019QS04), the National Natural Science Foundation of China (Grant No. 11574390), and the Strategic Priority Research Program of Chinese Academy of Sciences (Grant No. XDA 25051000).

†Corresponding author. E-mail: ghy@cumtb.edu.cn
‡Corresponding author. E-mail: lyj@aphy.iphy.ac.cn

© 2020 Chinese Physical Society and IOP Publishing Ltd

and BP effects are established for a cylindrically convergent interface.[23] It was found that large C_r would lead to severely nonlinear growth of perturbation. All these analyses mentioned above focused on the evolution of a single-mode perturbation at the initial stage. Haan[24] established the second-order WN theory for the multi-mode classical RT growth, the transition from linear to nonlinear is discussed. Xin *et al.*[25] numerically studied the evolution of two-mode ablative RT growth in a planar geometry. Mode-coupling of converging RM instability of dual-mode interface was numerical investigated by Zhou *et al.*,[26] the sign of perturbation amplitudes of the generated modes was discussed. Since the hydrodynamic instability in ICF implosion has entered a strong nonlinear phase,[27,28] constructing a WN model in a convergent geometry is practically meaningful, which helps us to at least improve understanding of the mode-coupling features. In this paper, the multi-mode BP growth in a cylindrical geometry is discussed.

This paper is organized as follows: Section 2 describes the theoretical model and derives the second-order solutions for BP growth. Section 3 displays the interface deformation and mode-coupling characteristics. Section 4 summarizes the major results and gives some conclusions.

2. Theoretical model

The two-dimensional cylindrical coordinate system (r,θ) is established. The r and θ are the radial and polar directions, respectively. Two incompressible, inviscid, irrotational fluids are separated by an interface with radius $R(t)$. When there is small perturbation at the interface, the perturbed interface can be expressed as $r=R+\eta(t,\theta)$, where $\eta(t,\theta)$ is the small perturbation displacement. The velocity potential ϕ is introduced and the corresponding fluid velocity follows the form $v=\nabla\phi$. In the subsequent discussion, the physical quantities of the interior fluid ($0<r<R$) and the exterior fluid ($R<r<\infty$) are denoted by the superscript "in" and "ex", respectively. The governing equations for this convergent system are

$$\nabla^2\phi^{\rm ex}=\nabla^2\phi^{\rm in}=0, \tag{1}$$

$$\frac{\partial\eta}{\partial t}+\frac{1}{r^2}\frac{\partial\eta}{\partial\theta}\frac{\partial\phi^{\rm in}}{\partial\theta}-\frac{\partial\phi^{\rm in}}{\partial r}=0 \ \ \text{at} \ \ r=R+\eta, \tag{2}$$

$$\frac{\partial\eta}{\partial t}+\frac{1}{r^2}\frac{\partial\eta}{\partial\theta}\frac{\partial\phi^{\rm ex}}{\partial\theta}-\frac{\partial\phi^{\rm ex}}{\partial r}=0 \ \ \text{at} \ \ r=R+\eta, \tag{3}$$

$$\begin{aligned}&\rho^{\rm in}\left\{\frac{\partial\phi^{\rm in}}{\partial t}+\frac{1}{2}\left(\frac{\partial\phi^{\rm in}}{\partial r}\right)^2+\frac{1}{2r^2}\left(\frac{\partial\phi^{\rm in}}{\partial\theta}\right)^2\right\}\\&-\rho^{\rm ex}\left\{\frac{\partial\phi^{\rm ex}}{\partial t}+\frac{1}{2}\left(\frac{\partial\phi^{\rm ex}}{\partial r}\right)^2+\frac{1}{2r^2}\left(\frac{\partial\phi^{\rm ex}}{\partial\theta}\right)^2\right\}\\&=f(t) \ \ \text{at} \ \ r=R+\eta,\end{aligned} \tag{4}$$

where $\rho^{\rm in}$ and $\rho^{\rm ex}$ are densities ($\rho^{\rm in}<\rho^{\rm ex}$) of two fluids. The $\phi^{\rm in}$ and $\phi^{\rm ex}$ are the velocity potentials associated with the fluid velocities and $f(t)$ is the function of time. Equation (1) describes the incompressible fluids. Equations (2) and (3) indicate the continuity of the normal velocity across the interface. The Bernoulli equation (4) describes the pressure continuity condition at the interface.

The interface perturbation can be expanded as

$$\eta(t,\theta)=\sum_m\eta_m(t)\,{\rm e}^{{\rm i}m\theta}, \tag{5}$$

where multi-mode perturbation growth is considered at the interface. We expand the amplitude $\eta_m(t)$ into the second order in a formal expansion parameter ε, namely,

$$\eta_m(t)=\varepsilon\eta_{1,m}(t)+\varepsilon^2\eta_{2,m}(t)+\cdots. \tag{6}$$

The velocity potentials of two incompressible fluids are expressed as

$$\phi^j=\phi_0(t,r)+\varphi^j, \tag{7}$$

where $j={\rm in},{\rm ex}$ and φ^j are the perturbed velocity potentials. Substituting Eq. (7) into the Laplace equation (1) and choosing the lowest order $O(\varepsilon^0)$, we can obtain

$$\phi_0(t,r)=R\dot{R}\ln r+a(t), \tag{8}$$

where $a(t)$ is an arbitrary function of time. The perturbed velocity potentials can also be expressed into the parameter ε as

$$\varphi^{\rm in}=\sum_m r^m\,{\rm e}^{{\rm i}m\theta}\left[\varepsilon\varphi^{\rm in}_{1,m}(t)+\varepsilon^2\varphi^{\rm in}_{2,m}(t)+\cdots\right], \tag{9}$$

$$\varphi^{\rm ex}=\sum_m r^{-m}\,{\rm e}^{{\rm i}m\theta}\left[\varepsilon\varphi^{\rm ex}_{1,m}(t)+\varepsilon^2\varphi^{\rm ex}_{2,m}(t)+\cdots\right], \tag{10}$$

the perturbed velocity φ^j already satisfies the Laplace equation (1). We substitute the perturbation displacement and velocity potentials in Eqs. (2)–(4) and perform Taylor expansion at $r=R$. Collecting the terms of the same power in ε and equating the coefficients of parameters ε and ε^2 to zero to construct the governing equations. The evolution of the perturbations are obtained by solving the successive equations.

At the first-order $O(\varepsilon)$, the equation for each fundamental mode is

$$\ddot{\xi}_{1,m}=A\frac{m}{R}\ddot{R}\xi_{1,m}, \tag{11}$$

where $\xi_1=\eta_1 R$, $A=(\rho^{\rm ex}-\rho^{\rm in})/(\rho^{\rm ex}+\rho^{\rm in})$ is the Atwood number. The overdot represents the derivative of time. Assuming $\gamma(t)^2=A\ddot{R}m/R$, the formula (11) is quite similar to the governing equation in planar geometry,[18] but with time-dependent growth rate here. The accelerationless case denotes the BP growth in the absence of acceleration, namely, $\ddot{R}=0$. Then, the equation is reduced to

$$\ddot{\xi}_{1,m}=0, \tag{12}$$

which describes linear growth of BP-type perturbation that is identical to Mikaelian's results,[29] where linear growth of RT

and RM instabilities in a multi-layer cylindrical shell is studied. In the following part, the purely BP growth is discussed for an uniformly convergent interface, namely, $R = R_0 - V_0 t$.

At the second-order $O(\varepsilon^2)$, the mode-coupling equation takes the form

$$\begin{aligned}\ddot{\xi}_{2,m} &= (Am-3)\frac{\dot{R}^2}{R^4}\sum_{m_2}\xi_{1,m_1}\xi_{1,m_2} \\ &\quad -(Am+1)\frac{1}{R^2}\sum_{m_2}\dot{\xi}_{1,m_1}\dot{\xi}_{1,m_2} - \frac{1}{R^2}\sum_{m_2}\xi_{1,m_1}\ddot{\xi}_{1,m_2} \\ &\quad +\frac{\dot{R}}{R^3}\sum_{m_2}(\dot{\xi}_{1,m_1}\xi_{1,m_2}+3\xi_{1,m_1}\dot{\xi}_{1,m_2}),\end{aligned} \tag{13}$$

where $\xi_2 = \eta_2 R$ and $m_2 = m - m_1$. As can be seen, mode-coupling process is related to the power of $1/R$, which means that mode-coupling behavior is affected by BP effects. The nonlinear mode-coupling would be more prominent in the process of implosion, especially for experiments with high convergence ratio design.

The BP growth for an uniformly convergent case is considered, $R = R_0 - V_0 t$. We investigate a case of two perturbation modes with mode numbers m_1 and m_2 at the initial stage. Second-order mode-coupling between two initial modes will generate other perturbations with mode numbers $2m_1$, $2m_2$, $m_1 + m_2$ and $m_1 - m_2$. The modes $2m_1$ and $2m_2$ are originated from the second harmonic generation and the modes $m_1 \pm m_2$ are from mode-coupling effect. The following initial conditions are adopted:

$$\eta_{1,m}(t=0) = \alpha_m, \qquad \dot{\eta}_{1,m}(t=0) = \dot{\alpha}_m. \tag{14}$$

The linear solutions for the multi-mode BP growth are

$$\eta_{1,m_1} = \alpha_{m_1} + \dot{\alpha}_{m_1} C_{\mathrm{r}} t, \qquad \eta_{1,m_2} = \alpha_{m_2} + \dot{\alpha}_{m_2} C_{\mathrm{r}} t, \tag{15}$$

where the convergence ratio is $C_{\mathrm{r}} = R_0/R$ and R_0 is the initial radius. The linear growth of the perturbation is related to the C_{r}, but independent of the Atwood number, which is different from the linear RT growth.

The second-order solutions for the sum and difference frequency mode are

$$\begin{aligned}\eta_+ &= (\alpha_{m_2}\dot{\alpha}_{m_1} + \alpha_{m_1}\dot{\alpha}_{m_2})\frac{1}{2R}\left[A(m_1+m_2)-1\right](C_{\mathrm{r}}-1)t \\ &\quad +\dot{\alpha}_{m_1}\dot{\alpha}_{m_2}\frac{1}{6R}\left[A(m_1+m_2)\left(C_{\mathrm{r}}^2-4C_{\mathrm{r}}\right)-3C_{\mathrm{r}}^2\right]t^2,\end{aligned} \tag{16}$$

$$\begin{aligned}\eta_- &= \frac{1}{2R}\left[A(m_1-m_2)(\alpha_{m_1}\dot{\alpha}_{m_2} - \alpha_{m_2}\dot{\alpha}_{m_1})\right. \\ &\quad \left.-(\alpha_{m_1}\dot{\alpha}_{m_2} + \alpha_{m_2}\dot{\alpha}_{m_1})\right](C_{\mathrm{r}}-1)t \\ &\quad +\dot{\alpha}_{m_1}\dot{\alpha}_{m_2}\frac{1}{6R}\left[A(m_1-m_2)\left(C_{\mathrm{r}}^2+2C_{\mathrm{r}}\right)-3C_{\mathrm{r}}^2\right]t^2,\end{aligned} \tag{17}$$

where the subscript $+$ and $-$ represent the $m_1 + m_2$ and $m_1 - m_2$, respectively. The explicit A, C_{r} and C_{r}^2 dependences of $\eta_{m_1 \pm m_2}$ are shown clearly. For a special case with mode number $m_1 = m_2$, the second harmonic generation for an initially single-mode perturbation is recovered.[22] As can be seen, the mode-coupling phenomenon is quite complicated in this convergent system. The phase of the second-order perturbation depends on the A, mode numbers and initial conditions. The phase changes will be analyzed in detail.

3. Results and discussion

We have already obtained the second-order WN solutions for the two-mode perturbation growth on a cylindrical interface that is imploded inward with an uniformly radial velocity. In this section, the two-mode perturbation growth caused purely by BP effects is analyzed. The mode-coupling process is discussed in some detail.

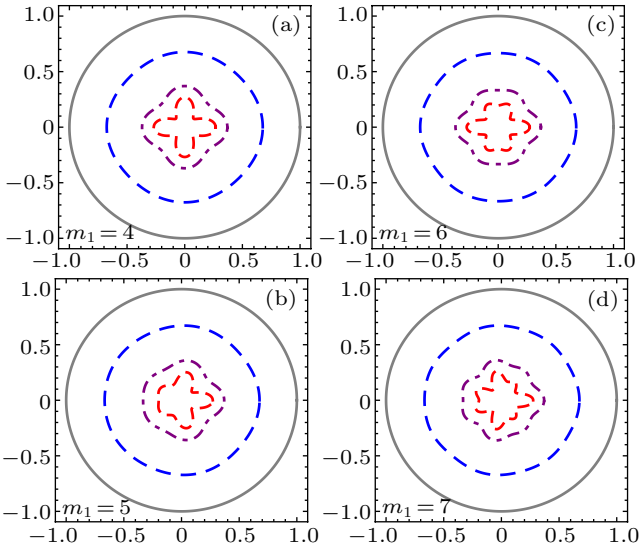


Fig. 1. Evolution of interfacial profiles for two-mode perturbations at $C_{\mathrm{r}} = 1$ (solid), 1.5 (dashed), 3 (dot-dashed) and 5 (dashed) with $A = 1.0$. The mode numbers are $m_1 = 4$ (a), 5 (b), 6 (c) and 7 (d), $m_2 = 4$. The initial velocity perturbations are $\dot{\alpha}_{m_1} = \dot{\alpha}_{m_2} = 0.01 V_0$.

Figure 1 displays the temporal evolution of the perturbed interface initiated by only velocity perturbation at convergence ratios $C_{\mathrm{r}} = 1$, 1.5, 3 and 5. The initial mode numbers are $m_1 = m_2 = 4$ for the single-mode results shown in Fig. 1(a), and $m_1 = 5, 6, 7$ for the multi-mode results in Figs. 1(b)–1(d). As can be seen, the convergent interface undergoes large deformation with time proceeding. For $A = 1$, the inward-going parts develop into the spike, and the outward-moving parts evolve into bubbles. In Fig. 1(a), the symmetry deformation of the interface is observed for a single-mode perturbation. However, the multi-mode perturbation leads to the irregular deformation of the interface. These multi-mode images are very similar to the experimental results of Hsing *et al.*,[10] where the irregular deformation of a cylindrical shell is measured, which comes from mode-coupling between an initial perturbation mode and an illumination asymmetry mode. As the wavelength $\lambda = 2\pi R/m$ with mode number m is decreased, the

nonlinear mode-coupling effect becomes important for large C_r. Convergence effect will reduce the threshold for mode-coupling to occur, as the perturbation wavelength decreases with convergence $\lambda \sim R/m$. As the interface moves without acceleration, the interface deformation is mainly determined by the inward and outward fluid motion.[22]

The normalized perturbation amplitudes for the initial two-mode perturbation at the interface are shown in Fig. 2. The initial perturbation modes are $m_1 = 20$ and $m_2 = 8$. During the implosion, other perturbation modes are generated through the mode-coupling. The modes $m = 16$ and 40 are from the second harmonic generation, the modes $m = 28$ $(m_1 + m_2)$ and $m = 12$ $(m_1 - m_2)$ are from mode-coupling of the initial two-mode perturbation. As can be seen, the second harmonic grows with negative phase, which has been discussed in Ref. [22]. The phases of difference frequency and the initial perturbation modes are the same, while the sum frequency grows with opposite phases. This means that low-mode perturbation generated from mode-coupling effect will grows with positive phase. In ICF implosion, low-mode growth at the inner interface will result in deformation of the hot-spot. Thus, special attention should be paid to growth of low-mode perturbation.

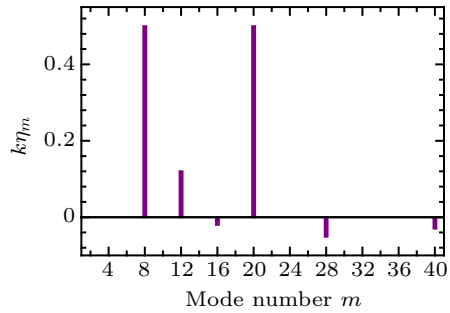


Fig. 2. Normalized perturbation amplitudes for the initial two-mode perturbation at convergent ratio $C_r = 3.5$. The equivalent wavenumber is $k = m/R$, the other parameters are $A = 1.0$, $m_1 = 20$, $m_2 = 8$ and $\dot{\alpha}_{m_1} = \dot{\alpha}_{m_2} = 0.01V_0$.

The amplitude of mode $m = 60$ from mode-coupling effect between mode $m_1 = 40$ and $m_2 = 20$ is displayed in Fig. 3. The dotted results are taken from Ref. [26], where the mode-coupling behaviors in converging Richtmyer–Meshkov instability on N_2/SF_6 interfaces are numerically considered. The initial interface position separating N_2 and SF_6 is $R_0 = 195$ mm, a cylindrical shock with Mach number of $M = 1.25$ is set at the perturbed interface. The incident shock encounters with the perturbed interface, resulting in a nearly uniformly convergent velocity (~91.0 m/s) of the shocked interface at the early stage. The temporal evolution of sum frequency $m = 60$ from mode-coupling between positive (negative) mode $m_1 = 40$ with $\alpha_{m_1} = \pm 0.2$ mm and a second mode $m_2 = 20$ with $\alpha_{m_2} = 1.5$ mm are shown in Fig. 3. The positive modes m_1 and m_2 generate the positive mode $m = 60$, the negative mode m_1 and positive m_2 generate the negative mode $m = 60$. These phenomena obtained from our WN theory of Eq. (16) quite agree with the numerical result of Zhou *et al.*[26] in the early stage.

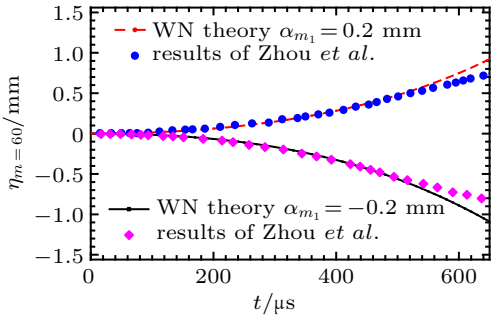


Fig. 3. Temporal evolution of mode $m = 60$ from initial two-mode perturbation ($m_1 = 40$, $m_2 = 20$). The solid and dashed lines are WN solutions to Eq. (16), the markers are the corresponding simulation results in Ref. [26] for $\alpha_{m_1} = \pm 0.2$ mm and $\alpha_{m_2} = 1.5$ mm.

Temporal evolution of perturbation mode $m = 20$ initialed by two-mode perturbations with $m_1 = 40$ and $m_2 = 20$ is displayed in Fig. 4. The initial perturbation amplitudes are $\alpha_{m_1} = -0.2$ mm and $\alpha_{m_2} = 1.5$ mm, the Atwood number is about -0.67. The dotted line denotes the numerical result of Zhou *et al.*,[26] the solid line is our WN theory. The detailed mode-coupling process can be obtained from our WN model. The amplitude of mode $m = 20$ contains two parts in the WN stage, namely, the growth of fundamental mode $m_1 = 20$ and the difference mode $(m_1 - m_2)$ generation from mode-coupling between m_1 and m_2 that expressed in Eq. (17). As can be seen, the analytical results are in good agreement with the numerical results in the early stage. The increasing discrepancy between the WN theory and the numerical results in the later time indicates the fact that the WN model presented in this paper is invalid, as the perturbation growth has exceeded the WN stage.

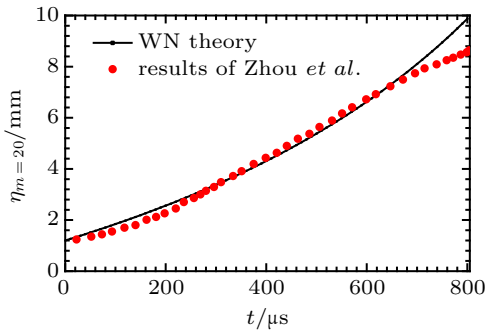


Fig. 4. Perturbation amplitude of mode $m = 20$ versus time for initial two-mode perturbation ($m_1 = 40$, $m_2 = 20$) with $\alpha_{m_1} = -0.2$ mm and $\alpha_{m_2} = 1.5$ mm. The solid line denotes our WN result, the dotted line is the numerical result taken from Ref. [26].

The mode-coupling behavior of two cases is illustrated in Fig. 5, where the convergent interface perturbed with similar wavelength (nearby modes) is shown in Fig. 5(a) and the case of dissimilar wavelength (dissimilar modes) perturbation is shown in Fig. 5(b). As can be seen, the phases of the

sum frequency mode η_+/λ and the difference frequency mode η_-/λ are opposite under the same conditions. The perturbation growth caused by the dissimilar modes is larger than that caused by nearby modes. As can be obtained from Eqs. (16) and (17), the perturbation amplitudes from mode-coupling are proportional to the perturbation modes. The case with nearby modes generates low-mode perturbations which lead to the smaller perturbation growth. The low-mode perturbation in ICF implosion is hard to control, as the low-mode perturbation is difficult to saturation.

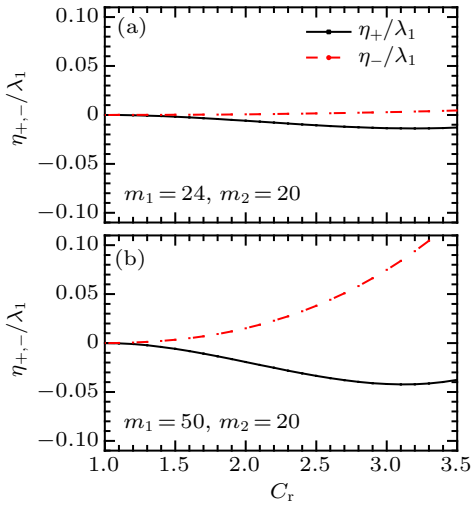


Fig. 5. The normalized amplitudes η_+/λ_1 (solid) and η_-/λ_1 (dashed) versus convergence ratio C_r for two nearby modes ($m_1 = 24$, $m_1 = 20$) (a) and dissimilar modes ($m_1 = 50$, $m_1 = 20$) (b) perturbations at the initial stage. The initial perturbations are $\dot{\alpha}_{m_1} = \dot{\alpha}_{m_2} = 0.01V_0$ and the Atwood number $A = 1.0$.

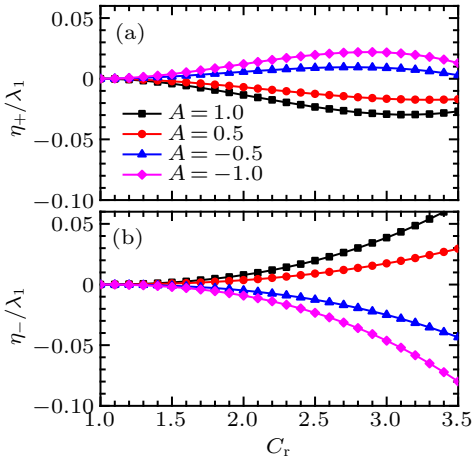


Fig. 6. The normalized amplitudes η_+/λ_1 (a) and η_-/λ_1 (b) for the Atwood numbers $A = 1.0$, 0.5, -0.5 and -1.0 with the initial perturbation $\dot{\alpha}_{m_1} = \dot{\alpha}_{m_2} = 0.01V_0$. The perturbation mode numbers are $m_1 = 40$ and $m_2 = 20$.

The Atwood number A dependence of mode-coupling amplitudes is investigated in Fig. 6. The $A = 1.0$ ($\rho^{in} = 0$) denotes the case that inside of the fluid interface is vacuum. The $A = -1.0$ ($\rho^{ex} = 0$) represents a special case where outside of the interface is vacuum. For $A < 0$, the mode-coupling between m_1 and m_2 generates a negative mode $m_1 - m_2$ with amplitude η_-. The amplitude η_+ of sum frequency mode $m_1 + m_2$ grows with positive phase. This phenomenon is identical to that in Ref. [26], where the phase of generated modes is analyzed numerically. However, the phases of both η_+ and η_- are all changed in π for $A > 0$ when compared with $A < 0$. The difference frequency amplitude η_- is greatly affected by A. The larger density ratio A at the interface results in the larger mode-coupling perturbation growth.

4. Conclusions

In summary, we have discussed the weakly nonlinear BP-type (purely converging effect) growth in cylindrical geometry. The governing equations for multi-mode coupling are derived. The second-order WN solutions for two-mode perturbations in cylindrically convergent geometry are obtained. The interface deformation and the mode-coupling behavior in WN regime are analyzed. The initial multi-mode perturbations lead to the irregular deformation of the convergent interface. The mode-coupling behavior in curved geometries relies on the Atwood number A, mode number m and convergence ratio C_r, which is different from that in planar geometries. Initial two dissimilar modes (dissimilar wavelength) lead to the larger perturbation growth than the perturbation case of two similar modes. The phase and amplitude of $\eta_\pm$ are affected by the Atwood number. The $A = -1.0$ at the interface will lead to severer perturbation growth than that for $A = 1.0$. The phase of generated modes from mode-coupling of fundamental mode can be easily obtained via the reduced WN formula. Although the typical ICF implosion targets are designed in a spherical geometry, the main feature of BP effects are captured at reduced levels in a cylindrical geometry,[29] which also enable experiments to utilize more directly validate models and benchmark simulations in convergent geometries.[30] Our WN model can be used to investigate the mode-coupling effect in converging Richtmyer–Meshkov instability of dual-mode interface.[26] The results present in this paper should be significant in understanding the nonlinear development of multi-mode perturbation growth in convergent geometry, as in most physical cases the problems cannot be described by a single mode. Furthermore, the present work could be valuable for verification of two-dimensional (2D) numerical codes.

References

[1] Lindl J D, Amendt P, Berger R L, Glendinning S G, Glenzer S H, Haan S W, Kauffman R L, Landen O L and Suter L J 2004 *Phys. Plasmas* **11** 339
[2] Wang L F, Ye W H, He X T, Wu J F, Fan Z F, Xue C, Guo H Y, Miao W Y, Yuan Y T, Dong J Q, Jia G, Zhang J, Li Y J, Liu J, Wang M, Ding Y K and Zhang W Y 2017 *Sci. China Phys. Mech. Astron.* **60** 055201
[3] Remington B A, Drake R P and Ryutov D D 2006 *Rev. Mod. Phys.* **78** 755
[4] Craxton R S *et al.* 2015 *Phys. Plasmas* **22** 110501
[5] Marocchino A, Atzeni S and Schiavi A 2010 *Phys. Plasmas* **17** 112703

[6] Rayleigh L 1882 *Proc. London Math. Soc.* **s1–14** 170
[7] Taylor G 1950 *Proc. R. Soc. Lond. A* **201** 192
[8] Bell G I 1951 *Los Alamos Scientific Laboratory Report* No. LA-1321
[9] Plesset M S 1954 *J. Appl. Phys.* **25** 96
[10] Hsing W W, Barnes C W, Beck J B, Hoffman N M, Galmiche D, Richard A, Edwards J, Graham P, Rothman S and Thomas B 1997 *Phys. Plasmas* **4** 1832
[11] Hsing W W and Hoffman N M 1997 *Phys. Rev. Lett.* **78** 3876
[12] Amendt P, Colvin J D, Ramshaw J D, Robey H F and Landen O L 2003 *Phys. Plasmas* **10** 820
[13] Wang X G, Sun S K, Xiao D L *et al.* 2019 *Chin. Phys. B* **28** 035201
[14] Zhai Z G *et al.* 2018 *Proceedings of the Institution of Mechanical Engineers, Part C: Journal of Mechanical Engineering Science* **232** 2830
[15] Ding J C *et al.* 2017 *Phys. Rev. Lett.* **119** 014501
[16] Epstein R 2004 *Phys. Plasmas* **11** 5114
[17] Velikovich A L and Schmit P F 2015 *Phys. Plasmas* **22** 122711
[18] Guo H Y *et al.* 2017 *Phys. Plasmas* **24** 112708
[19] Guo H Y, Wang L F, Ye W H, Wu J F and Zhang W Y 2018 *Chin. Phys. B* **27** 055205
[20] Zhang J, Wang L F, Ye W H, Wu J F, Guo H Y, Zhang W Y and He X T 2017 *Phys. Plasmas* **24** 062703
[21] Wang L F, Wu J F, Ye W H, Zhang W Y and He X T 2013 *Phys. Plasmas* **20** 042708
[22] Wang L F, Wu J F, Guo H Y, Ye W H, Liu J, Zhang W Y and He X T 2015 *Phys. Plasmas* **22** 082702
[23] Guo H Y, Wang L F, Ye W H, Wu J F and Zhang W Y 2018 *Chin. Phys. Lett.* **35** 055201
[24] Haan S W 1991 *Phys. Fluids B* **3** 2349
[25] Xin J, Yan R, Wan Z H, Sun J, Zheng J, Zhang H, Aluie H and R. Betti R 2019 *Phys. Plasmas* **26** 032703
[26] Zhou Z B, Ding J C, Zhai Z G, Wan C and Luo X S 2019 *Acta Mech. Sin.*
[27] Weber C R, Clark D S, Cook A W *et al.* 2015 *Phys. Plasmas* **22** 032702
[28] Clark D S, Marinak M M, Weber C R *et al.* 2015 *Phys. Plasmas* **22** 022703
[29] Mikaelian K O 2005 *Phys. Fluids* **17** 094105
[30] Sauppe J P, Haines B M, Palaniyappan S, Bradley P A, Batha S H, Loomis E N and Kline J L 2019 *Phys. Plasmas* **26** 042701